

Chapter 17

Thermal Infrared Remote Sensing of Geothermal Systems

Christian Haselwimmer and Anupma Prakash

Geophysical Institute, University of Alaska Fairbanks, 903 Koyukuk Drive, Fairbanks, Alaska, 99775, USA. E-mail: chha@gi.alaska.edu

Abstract

In areas of anomalously high crustal heat flow, geothermal systems transfer heat to the Earth's surface often forming surface expressions such as hot springs, fumaroles, heated ground and associated mineral deposits. Geothermal systems are increasingly important as sources of renewable energy, natural wonders often afforded protected status, and their study is relevant to monitoring deeper magmatic processes. Thermal infrared (TIR) remote sensing provides a unique tool for mapping the surface expressions of geothermal activity as applied to the exploration for new geothermal power resources and long term monitoring studies. In this chapter, we present a review of TIR remote sensing for investigations of geothermal systems. This includes a discussion on the applications of TIR remote sensing to the mapping of surface temperature anomalies associated with geothermal activity, measurement of near-surface heat fluxes associated with these features as input into monitoring and resource assessment, and for mapping of surface mineral indicators of both active and recently active hydrothermal systems.

17.1 Introduction

Geothermal systems occur in regions of anomalously high crustal heat flow that may be related to the presence of young igneous bodies or hot rocks located deeper in the crust (Rybach, 1981; DiPippio, 2005). This elevated geothermal heat is normally transferred to the surface by the convection of ground waters that forms hydrothermal systems: surface waters circulate to depth where they are heated and rise to the surface via a subterranean 'plumbing system' of closely spaced fractures or other zones of permeable rock (Figure 1). If rising hot waters reach the surface then characteristic geothermal features such as hot springs, fumaroles, and geysers may form (Heasler et al., 2009).

When the heat contained within fluid filling fractures and permeable rocks is sufficiently accessible, this energy can be exploited for power generation or direct use (geothermal energy). Around the world, geothermal energy accounts for approximately 10,700 megawatts-electric (MWe) of power production with estimates of the potential resource ranging from 35 - 2,000 gigawatts-electric (Fridleifsson et al., 2008). In areas of high crustal heat flow geothermal power offers an attractive low-carbon alternative to traditional fossil-fuel based energy and as such there is increasing interest in the exploration and development of new geothermal resources such as in the Great Basin of the western United States.

Studying surface geothermal activity and heat loss associated with magmatic-related systems is important for monitoring of subsurface igneous activity. For example, the abundant geothermal features at Yellowstone National Park are the surface expressions of the largest active volcanic system in North America. Surface hydrothermal activity at Yellowstone has changed over time indicating variations in geothermal system activity that may be in-turn related to changes in magmatic activity (Heasler et al., 2009). In addition, the monitoring of geothermal activity has a role to play in efforts to conserve geothermal systems that are of cultural significance or are economically important tourism destinations; with the increasing development of geothermal resources there is potential to negatively impact these sites (Bromley et al., 2010).

Thermal infrared (TIR) remote sensing provides data with synoptic coverage for investigating the surface manifestations of geothermal systems as applied to both geothermal energy exploration and also for more fundamental research and monitoring. TIR remote sensing provides a method for rapid mapping and quantifying surface geothermal features in support of exploration and assessment of new resources (Hodder, 1970; Mongillo, 1994; Allis et al., 1999; Mongillo and Graham, 1999; Eneva et al., 2006; Kratt et al., 2006; Kratt et al., 2006; Coolbaugh et al., 2007; Eneva et al., 2007; Rockwell and Hofstra, 2008; Kienholz et al., 2009; Littlefield and Calvin, 2009; Scherer et al., 2009; Taranik et al., 2009; Littlefield and Calvin, 2010; Haselwimmer et al., 2011; Reath and Ramsey, 2011). In addition, TIR data can be used to monitor these features at developed reservoirs that may provide indications of unsustainable resource extraction (Allis, 1980; Bromley et al., 2010) or provide estimates of surface heat loss as input to reservoir models (Bromley et al., 2011). The use of TIR data to map and quantify surface geothermal features also supports long term monitoring of magmatic-related and/or protected systems (Watson et al., 2008; Heasler et al., 2009; Seielstad and Queen, 2009).

In this chapter, we present a review of TIR remote sensing for studying geothermal systems. This includes a discussion on the application of TIR remote sensing to the mapping of surface temperature anomalies associated with geothermal activity, the measurement of near-surface heat fluxes associated with these features

as input for monitoring and resource assessment, and mapping of surface mineral indicators of both active and recently active hydrothermal systems.

17.2 Surface manifestations of geothermal systems

Geothermal systems display surface manifestations when there is sufficient permeability that enables geothermal waters to rise to and outflow at the surface (DiPippio, 2005). Depending upon the temperature and outflow rate of geothermal fluids, discrete surface features can include hot springs, seeps, fumaroles, geysers, mud-pots, and steam-heated pools. More widespread areas of heated or steaming ground occur due to conductive heat loss above outflow zones containing geothermal fluids and as a result of the direct convective heating from steam or hot water (Rybach, 1981; DiPippio, 2005) (Figure 1). The temperatures of geothermal fluids show a considerable range: low-temperature systems ($<90^{\circ}\text{C}$) are referred to as spring-dominated as outflow occurs via hot springs or seeps. Systems with intermediate ($90\text{-}150^{\circ}\text{C}$) and high ($150\text{-}240^{\circ}\text{C}$) temperature fluids are vapor-dominated as these fluids boil in the subsurface, due to lowering hydrostatic pressure, producing steam or water/steam dominated surface features such as fumaroles, geysers, and steaming ground (Rybach, 1981) (Figure 1).

Subsurface geothermal fluids will dissolve minerals in the rocks along the fluid circulation paths that they travel. This can lead to the development of new alteration minerals, such as clays, zeolites, and calcite and the removal of minerals as the dissolved load in geothermal fluids (Glassley, 2010). Mineral alteration in geothermal systems reflects the temperature and chemistry of geothermal waters, as well as the composition of the surrounding bedrock. As geothermal waters cool and move away from the heat source, the dissolved mineral load will start to precipitate. In some cases, surface discharge of these fluids forms mineral deposits as the waters cool and the dissolved load precipitates that include: 1) siliceous sinters encompassing various forms of silica deposited by high-temperature fluids ($>175^{\circ}\text{C}$); 2) travertine, which is mainly calcium carbonate deposited by lower temperature geothermal fluids; 3) borates, sulfates, and chlorides (Glassley, 2010).

Many geothermal systems do not display active surface expressions and are termed 'blind' systems. These may occur when geothermal fluids cool before they reach the surface or are not able to reach the surface due to lateral flow in deeper aquifers or the presence of impermeable capping layers (Figure 1). Considerable effort has focused on the exploration for blind geothermal resources. Coolbaugh and Shevenell (2004) estimate that these undiscovered geothermal resources in the State of Nevada significantly exceeds the known resources.

(Insert Figure 1)

17.3 Mapping geothermal surface temperature anomalies

TIR remote sensing data can be used to map and quantify temperature anomalies associated with surface geothermal features such as hot springs, geysers, fumaroles, and heated ground. This approach has been used as a cost-effective tool for geothermal exploration over large areas enabling subsequent selection of targets for further exploration using ground-based surveys (Hodder, 1970; Lee, 1978; Mongillo, 1994; Haselwimmer et al., 2011). In addition, TIR remote sensing has been applied to the cataloguing and long-term monitoring of thermal features associated with developed and protected geothermal systems (Mongillo, 1994; Seielstad and Queen, 2009).

Much of the published research on the use of TIR remote sensing for mapping surface temperature anomalies has focused on the use of airborne thermal imagery acquired with broadband (Hodder, 1970; Lee, 1978; Haselwimmer et al., 2011) or multispectral instruments (Mongillo, 1994; Seielstad and Queen, 2009). High resolution airborne thermal data (i.e. < 5 m pixels) enables detailed mapping of surface geothermal features that may be small in size or display limited temperature contrast with surrounding non-geothermal surfaces.

Hodder (1970) acquired pre-dawn broadband thermal imagery (in the 8-14 μm wavelength region) in the region of Long Valley and the Salton Sea, California, USA to map surface geothermal anomalies. Simple visual analysis and application of thresholds to the thermal data provided the basis for identification of hot waters at springs and heated ground overlying faults providing potential indicators of geothermal upwelling zones. Lee (1978) also exploited pre-dawn airborne thermal imagery to map geothermal features in the Black Rock Desert area of Nevada, USA. The thermal data provided an effective method for inventorying known geothermal features and mapping many previously unreported hot springs and related fractures.

Mongillo (1994) utilized a GEOSCAN MkII aerial scanner to acquire 3 m spatial resolution, multispectral TIR data (6 bands in the 8.4 - 11.6 μm wavelength region) during 1992 and 1993 for a 100 km^2 area covering the Waimangu-Waiotapu geothermal region with the aim of mapping and monitoring surface geothermal features. The acquired thermal data was empirically calibrated using in-situ measurements of non-geothermal water bodies and the resultant surface temperature data was visually interpreted. The results enabled mapping of all the known and many previously unidentified geothermal features including hot springs, hot ground, and thermal seeps into lakes. The results clearly outlined that geothermal features at the Waiotapu field occur along lineations providing strong evidence for a fault controlled upflow/outflow of geothermal fluids. Comparison of the results from different years indicates that a large hot spring appeared in the Waimangu

geothermal field between the two survey dates, which suggests the potential of TIR data for monitoring temporal changes in geothermal surface features.

Seielstad and Queen (2009) used airborne multispectral midwave- (MWIR: 3.6 – 5.1 μm) and longwave-infrared (8.1 – 12.4 μm) data acquired with an ADS SpectraView and US Fish and Wildlife Service (USFWS) ‘Firemapper’ system respectively to map and monitor thermal features in the Norris Geyser Basin, Yellowstone National Park. The ~1-3 m spatial resolution data acquired during daytime and nighttime surveys in 2005 and 2006 were calibrated to surface kinetic temperature values with an empirical correction using in-situ temperature measurements. The TIR data enabled detailed mapping of surface geothermal phenomena in the Norris Geyser Basin including discrete features such as hot springs and geysers as well as ‘background’ areas of sinter and heated ground. Seielstad and Queen (2009) used the data to broadly delineate the geographic boundaries of the Norris Geyser Basin that was previously poorly defined. In addition, more detailed mapping of a series of sub-basins within the Norris Geyser Basin was also undertaken. For the 2005 data, snow fall prior to the survey facilitated the mapping of geothermal ground that was snow free in contrast to the surrounding snow covered non-geothermal areas.

Haselwimmer et al. (2011) acquired ~1m spatial resolution airborne thermal imagery using a broadband FLIR systems A320 camera (operating in the 7.5 – 13 μm wavelength region) during fall and winter-time surveys over Pilgrim Hot Springs located near Nome in Western Alaska. The TIR data was calibrated to surface temperature values using a combination of MODTRAN and an empirical adjustment with in-situ temperature measurements. Georeferencing of the data was undertaken using the GPS positions of low-emissivity thermal blankets that provided distinctive ‘cold’ targets in the TIR imagery. The mosaicked and calibrated data enabled the detailed mapping of known and previously unmapped geothermal features including hot springs and pools, thermally anomalous ground (Figure 2), and ice free-areas on the nearby Pilgrim River that indicated geothermal outflow at a distance from the known spring’s site. In particular, this data provided very detailed information on the location and temperature of hot springs and sources of more diffuse geothermal outflow that were not obvious from field investigations. Mapping these features indicated two broad swaths of generally high temperature and low temperature springs that suggests an elongated zone of permeability, possibly related to the presence of an N-S oriented fault. The 2011 TIR data, acquired during Alaskan winter-time conditions, was effective for mapping areas of heated ground that appeared as areas of anomalous snow-melt. These areas did not display anomalous surface temperatures in the fall 2010 survey, due to the presence of vegetation cover or the effects of solar heating.

(Insert Figure 2)

Although coarse spatial resolution satellite thermal sensors (60-90 m pixels), such as Landsat or ASTER, have limited potential for detailed mapping of discrete geothermal features a number of studies have exploited these datasets for broader scale detection of geothermal anomalies (Coolbaugh et al., 2007; Eneva et al., 2007; Eneva and Coolbaugh, 2009; Kienholz et al., 2009). These studies have commonly applied data processing techniques to enhance and detect what may be subtle surface temperature anomalies. At the resolution of satellite TIR data, pixels corresponding to geothermal areas normally record a mixture of emitted radiance from geothermal sources as well as from background non-geothermal surfaces. This acts to reduce the measured temperature of pixels corresponding to geothermal sources. When this is compounded by other environmental factors such as land surface type, topography, albedo, and thermal inertia then it can be difficult to locate geothermal anomalies with confidence.

Kienholz et al. (2009) used multi-temporal Landsat thermal data to map geothermal anomalies on the Island of Akutan located on Alaska's Aleutian Arc. Twelve summertime cloud-free scenes were selected from the Landsat archive corresponding to acquisitions over Akutan Island between 1985 and 2008. The Landsat thermal bands were calibrated to surface kinetic temperature and an image stacking procedure was used to highlight persistent surface temperature anomalies and subdue background transient temperature effects associated with local scene specific conditions. As some persistent temperature effects remained after stacking, the results were further classified based upon elevation, slope, vegetation type and geology. This processing strategy mapped the locations of the known fumarole field and thermal springs and also revealed three new distinct regions of surface thermal anomalies providing targets for field investigations.

A number of studies have used ASTER data to detect surface geothermal anomalies by minimizing the temperature variations caused by diurnal solar heating effects (Coolbaugh et al., 2007; Eneva et al., 2007; Eneva and Coolbaugh, 2009). Factors such as albedo, topographic slope/aspect, emissivity, and thermal inertia affect the temperature changes of Earth surfaces over the 24 hour temperature cycle (Taranik et al., 2009). These variations potentially mask subtle temperature anomalies related to subsurface geothermal heating in TIR data. An example of this is the main sinter terrace at Steamboat Springs, Nevada, USA, where pre-dawn TIR images do not detect a thermal anomaly in spite of their being numerous fumaroles present at the site (Taranik et al., 2009). This is explained by the low albedo of the sinter that reflects much of the sun's energy during the day, and its low thermal inertia, which causes it to cool off rapidly at night.

In a study of Brady's Hot Springs, Nevada, USA, Coolbaugh et al. (2007) processed a day/night pair of ASTER scenes (acquired on the same date) to minimize the effects of diurnal heating. Using the ASTER Level 2 on-demand surface kinetic temperature product (AST08), Coolbaugh et al. (2007) applied corrections for albedo, topographic slope, and thermal inertia based upon a simplified

heat energy model describing net surface radiation flux. Surface temperature variations related to differences in albedo were corrected using the ASTER visible and infrared bands and a Digital Elevation Model (DEM) was used to correct for the effects of topographic slope and aspect. The impact of thermal inertia on surface temperature was corrected using mean surface temperatures for the diurnal cycle derived by adjusting the average of the ASTER day/night pair using field measurements of ground surface temperatures made over the same 24-hour period (Coolbaugh et al., 2007). The resultant processed image (Figure 3) shows that background variations in temperature were reduced by 30-50% whilst the intensity values of geothermal anomalies were retained. This made it easier to distinguish geothermal activity from false thermal anomalies associated with variations in topography, rock/soil types, and non-thermal springs (Coolbaugh et al., 2007).

(Insert Figure 3)

Eneva et al. (2006) applied a simplified version of the method used by Coolbaugh et al. (2007) to map thermal anomalies in the Coso geothermal field, California, USA, also using a daytime/nighttime pair of ASTER images. In this study, the correction for thermal inertia effects was simplified due to the lack of field measurements of surface temperatures over the 24 hour cycle. In spite of this, the processed ASTER data was effective in enhancing some thermal anomalies and suppressing false positives.

Whilst the method of Coolbaugh et al. (2007) is effective at enhancing geothermal anomalies and suppressing many non-geothermal effects, there are several limitations of this approach. The method uses a simplified surface energy balance model that does not account for sensible and latent heat losses. The assumption of radiation being the main control on heat loss is valid for dry non-vegetated ground, such as is commonly encountered in the Great Basin of the Western US, but will not hold for areas of moist ground or vegetation where heat loss will be dominated by evaporation and transpiration (Coolbaugh et al., 2007). Eneva and Coolbaugh (2009) describe how elevation and temperature inversions may effect ASTER surface temperature values and that these factors should ideally be taken into account when processing thermal images to enhance geothermal anomalies.

17.4 Quantifying geothermal heat fluxes

Hot springs, fumaroles, mud-pots, and steaming or heated ground are the surface expressions of conductive and convective heat loss from geothermal systems. As described in the previous section, TIR remote sensing provides a means to map the spatial distribution, extent, and temperature of these features that can in turn be used to estimate the conductive and convective heat loss near the surface. The measurement of this surface heat loss (aka. the near surface Geothermal Heat Flux

– GHF) is important for long-term monitoring of geothermal systems (Heasler et al., 2009), can be used to assess the resource potential of undeveloped geothermal reservoirs (Wisian et al., 2001), and also be applied to monitoring and modeling of developed resources (Allis, 1980).

Although TIR remote sensing has been widely used to monitor heat loss from volcanoes (e.g. Pieri and Abrams, 2004; Carter et al., 2008), it has been applied less in the monitoring of geothermal or hydrothermal systems. Much of this work has focused on Yellowstone National Park. Airborne thermal surveys of the Norris Geyser basin acquired between 2002 and 2006 have been used to map surface geothermal activity and monitor the associated GHF (Seielstad and Queen, 2009) (Figure 4). To quantify GHF Seielstad and Queen (2009) used the Stefan-Boltzmann equation to calculate the radiative component of heat loss from airborne surface temperature data:

$$M = \sigma T^4$$

where M is radiative heat loss in units of W m^{-2} , σ is the Stefan-Boltzmann constant (5.667×10^{-8}), and T is the surface radiant temperature in Kelvin. For geothermal features, the radiative heat loss was corrected for the background flux using the average radiative flux from non-geothermal areas. This adjustment removed the background radiation from surfaces at ambient temperature to yield just the geothermal component and also had the effect of normalizing GHF estimates from the different survey dates. Rather than using a single value for the background flux, this was calculated for each land cover type. For example, the background flux of vegetation outside the geothermal areas was used to correct flux values of vegetated patches within elevated temperature areas. Using this approach Seielstad and Queen (2009) estimated the GHF for Norris Geyser Basin from 2002, 2005, and 2006 airborne thermal data to be 136, 137, and 114 megawatts of thermal energy (MW_{th}), respectively. Given the uncertainty in background flux, combined with noise from calibration and emissivity separation, Seielstad and Queen (2009) concluded that there was no detectable change in the GHF over this period. Seielstad and Queen (2009) also highlighted that from a synoptic perspective most of the geothermal heat loss did not occur from discrete high temperature features, such as hot springs or fumaroles, but from the more spatially extensive areas of ‘background’ thermally anomalous ground.

(Insert Figure 4)

Watson et al. (2008) mapped a lower bound for the surface GHF for Yellowstone National Park using Landsat 7 ETM+ data by calculating a residual terrestrial emittance anomaly (TEA) for snow free areas using a surface energy balance model. In this model, terrestrial emittance (M_{terr}) represents one component in a system of fluxes at the surface that balances heat losses against heat gains:

$$M_{terr} + H_S + H_L + H_Q = GHF + S - R + M_{down} - M_{refl} + H_p + \Delta$$

where S and R are incident and reflected total solar radiation, H_S and H_L are sensible and latent heat exchange with the atmosphere, H_p and H_Q are advected heat flux in precipitation and runoff, and Δ accounts for change in storage in the subsurface. Based upon a simplified version of this surface energy balance equation Watson et al., (2008) calculated the TEA as the residuals of a multiple linear regression model linking surface heat losses to the surface temperature and non-geothermal heat gains to elevation and absorbed solar radiation. The latter was derived from a simple model of solar irradiation of hilly terrain, and surface albedo estimated from summation of the non-thermal bands of the ETM+ data (Watson et al., 2008). Using this approach, Watson et al. (2008) mapped the TEA with values ranging from 0 W m^{-2} up to 94 W m^{-2} throughout Yellowstone National Park that clearly discriminated geothermal from non-geothermal areas. The TEA results were validated against values of GHF calculated from the inversion of a snowpack model. Comparison of TEA and GHF values showed good agreement although the TEA was consistently lower and therefore provided a lower bound on GHF for the Yellowstone geothermal system (Watson et al., 2008).

Vaughan et al. (2011) analyzed ASTER and MODIS thermal data for Yellowstone National Park acquired in the 2000 to 2010 period with the aim of monitoring surface geothermal activity by calculating the radiant component of heat loss for geothermal areas. This study aimed to identify normal background thermal changes so that significant or abnormal changes related to geothermal activity could be recognized. Frequent but low resolution (1km) MODIS data were analyzed and a method for subtracting the seasonal variation in background thermal flux was developed. Analysis of the MODIS data using this method indicated that all of the thermal areas were stable during the 2000 to 2010 period. Vaughan et al. (2011) used higher spatial resolution but less frequently acquired ASTER thermal data to calculate radiant GHF for the whole of Yellowstone National Park that resulted in an estimate of $\sim 2 \text{ GW}_{th}$ (gigawatts thermal energy), which is somewhat lower than the value of 4-6 GW_{th} calculated from geochemical methods.

A number of studies have applied airborne TIR remote sensing to estimate geothermal heat flow in support of the assessment of new geothermal prospects and monitoring of existing developed resources (Allis et al., 1999; Mongillo and Graham, 1999; Bromley et al., 2011; Haselwimmer and Prakash, 2011). Allis et al., (1999) analyzed pre-dawn airborne thermal imagery over the Dixie Valley (Nevada, USA) and Wairakei (New Zealand) developed geothermal fields with the aim of mapping the near-surface conductive component of GHF. Using in-situ shallow temperature measurements and a fixed value of soil thermal conductivity ($\sim 0.5 \text{ W/m}^\circ\text{C}$), Allis et al. (1999) established an empirical relationship between surface conductive heat flow and thermal infrared surface temperature values for areas of heated ground. Although this approach provided a simple method of con-

verting TIR imagery into surface heat flow maps, Allis et al. (1999) point out a number of significant limitations and uncertainties with this approach: 1) the 'ambient' temperature of non-geothermal ground must be in the range 15-20°C; 2) the surface soil temperature for geothermally heated ground must be less than 90°C so that steam does not affect TIR-derived temperature values; 3) the effects of solar heating, emissivity or rainfall should be minimized. Mongillo and Graham (1999) applied the same empirical approach to estimate conductive heat flow using airborne thermal data acquired over part of the Taupo geothermal area in New Zealand. Moreover, they mapped anomalous geothermal features with temperatures > 2°C above background and estimated a conductive heat flow of ~2.5 MW_{th} that was supporting these features.

Bromley et al. (2011) used airborne thermal imagery to estimate the heat flux associated with steaming ground at the Wairakei-Tauhara geothermal system in New Zealand. Three different approaches were applied to the airborne thermal data to calculate the heat flux associated with steam-heated ground:

1. For thermally anomalous ground, areas of steam heating were delineated (based upon a dip in expected surface temperature related to the presence of steam) and surface temperature values for these areas were used to derive boiling point depths that then formed the basis of heat flux estimates using an empirical relationship.
2. For areas of steam-heating, the heat flux was directly calculated using an empirical relationship between heat flux and the temperature difference between steam-heated ground and ambient atmosphere.
3. For areas of steam-heated ground, the thermal flux was calculated directly from the surface temperature data by accounting for radiative, convective and conductive heat fluxes from anomalously hot ground to the air.

Bromley et al. (2011) produced consistent values for heat flux associated with steam heated ground of 35.6, 33.4, and 32.4 MW_{th} respectively for the three different methods. When these measurements were coupled with heat flux estimates from springs, seeps, and craters a total heat flux of ~86 MW_{th} was calculated for the Wairakei-Tauhara area.

Haselwimmer and Prakash (2011) used airborne thermal imagery acquired over Pilgrim Hot Springs during two surveys to quantify the convective heat flux and corresponding outflow rate of surface geothermal fluids as input into the resource assessment of this undeveloped system. The convective geothermal heat flux associated with surface geothermal fluids (i.e. hot springs, hot pools) was estimated from calibrated TIR surface temperature data for areas of hot water by accounting for radiative, evaporative, and sensible heat losses as well as heat gains from the geothermal source, incoming solar and atmospheric TIR radiation. Using this approach, the total convective heat flux supporting geothermal fluid outflow was

conservatively estimated at ~ 3.65 MW_{th}, which corresponded to a flow rate of ~ 195 gallons per minute (GPM), assuming a fixed hot spring temperature of 81°C. This value for the hot spring heat flux was higher than previous estimates of ~ 2 MW_{th} of energy that was derived from in-situ measurements of the flow rate of the hot springs. Given the difficulty in determining the flow rate of diffuse hot springs/seeps and the lack of well confined outflow at Pilgrim Hot Springs, Haselwimmer and Prakash (2011) suggest that the airborne thermal imagery provides a more realistic estimate of the total hot spring heat flux and flow rate.

17.5 Mapping geothermal indicator minerals

Surface minerals commonly deposited or produced from geothermal waters or hydrothermal alteration have spectral absorption features in the visible to thermal infrared wavelength regions related to electronic and molecular vibrations. These spectral absorption features provide the basis for mapping of these materials using multispectral and hyperspectral remote sensing that can map both active and blind geothermal systems (Kratt et al., 2006).

Numerous studies have exploited the visible/near-infrared to shortwave infrared (VNIR/SWIR) wavelength region for mapping hot spring deposits and related bedrock alteration products using multispectral (Kruse, 2002; Hellman and Ramsey, 2004; Kratt et al., 2006) and hyperspectral (Hellman and Ramsey, 2004; Nash et al., 2004; Kratt et al., 2006; Littlefield and Calvin, 2010) remote sensing. In the 0.4 – 2.5 μm wavelength region, mineral spectral absorption features record the interaction of light with cations (Fe, Mg, Al), and anions (OH, H₂O, CO₃) in mineral structures (Hunt, 1977). Minerals displaying diagnostic absorption features that occur in and typify hydrothermal alteration systems include hydroxyl bearing clays, sulfates, carbonates, and sinters (Huntington, 1996).

In the TIR wavelength region, mineral groups including silicates, carbonates, sulfates, phosphates, and hydroxides display diagnostic spectral absorption features (reststrahlen features) that appear as emissivity minima, which are related to fundamental molecular vibrations within different anion groups such as CO₃, SO₄, PO₄, and SiO₄. Further, the stretching and bending modes of major cations (e.g. Mg, Fe, Ca, Na) provide the basis for detailed discrimination of mineral species and excellent identification of specific silicate and carbonate minerals (Christensen et al., 2000). At TIR wavelengths the spectral emission properties of mixed materials can be considered to represent the linear combination of the constituents spectra weighted by their areal proportion (Hapke, 1993). This provides the basis for quantitative estimation of the modal compositions of mixed thermal emission spectra based upon approaches such as linear spectral deconvolution (Ramsey and Christensen, 1998). Typical minerals deposited by hot springs or associated with hydrothermal alteration display unique spectral emission features in

the thermal infrared (Figure 5). Although many minerals of importance for geothermal exploration do display distinctive absorption features in the VNIR/SWIR region, emission data provides capabilities in particular for discrimination of silicate and carbonate minerals. The synergistic use of VNIR/SWIR and TIR spectral data provides the greatest potential for unambiguous mapping of specific mineral occurrences in support of geothermal exploration (Riley et al., 2008).

Most research on the application of thermal emission data for mapping geothermal indicator minerals has focused on the use of the airborne SEBASS (the Spatially Enhanced Broadband Array Spectrograph System) and MASTER (MODIS-ASTER Airborne Simulator) instruments particularly for study sites located in the Great Basin of the Western United States. SEBASS is an airborne pushbroom hyperspectral imaging spectrometer designed by the Aerospace Corporation that acquires 256 channels of data, 128 in the 2.5 – 5.2 and 128 in the 7.5 – 13.5 μm wavelength regions (Hackwell et al., 1996). The MASTER system was designed by the NASA AMES Research Center and JPL to simulate the MODIS and ASTER instruments on board the NASA Terra satellite (Hook et al., 2001). MASTER acquires multispectral TIR imagery using 15 and 10 bands covering the 3.1 – 5.2, and 7.8 – 12.9 μm wavelength regions, respectively.

Vaughan et al. (2005) have made the most significant contribution to the geothermal remote sensing literature in their study of the Steamboat Springs active geothermal system in Nevada, USA. This study used high spatial resolution MASTER (5 m) and SEBASS (2 m) thermal emission data acquired on airborne surveys over Steamboat Springs during September 1999. The at-sensor long-wave infrared radiance data for the two instruments were atmospherically corrected using the MODTRAN radiative transfer model (Berk et al., 1989) and the ISAC (In Scene Atmospheric Compensation) (Johnson, 1998; Vaughan et al., 2003) algorithm, respectively, followed by a temperature-emissivity separation algorithm, TeS, (Gillespie et al., 1998) and a emissivity-normalization (Kealy and Gabell, 1990) algorithm. Mineral mapping using SEBASS and MASTER thermal emission data were undertaken using the commonly applied ‘hour-glass’ processing workflow (Kruse et al., 2003) that couples procedures for image data reduction (Minimum Noise Fraction transformation), end-member extraction (Pixel Purity Index), and spectral classification (Spectral Angle Mapper / Matched Filter). The mineralogy of mapped end-member classes were interpreted with reference to the spectra of pure minerals from the ASTER (Baldrige et al., 2009) and Arizona State University (ASU) (Christensen et al., 2000) spectral libraries. For the SEBASS results, linear mixtures of pure mineral library spectra were calculated to approximate the SEBASS end-member spectra and identify the presence of the dominant mixed components. The results of mineral mapping with MASTER data enabled broad discrimination of silica- and sulfate-rich ground (mapped as quartz, alunite, or opal) representing active geothermal areas and clay-rich ground (mapped as kaolinite or montmorillonite) corresponding to areas of hydrothermal alteration. The spectral resolution of the SEBASS data enabled more detailed discrimination of

pure minerals and assemblages including opal, quartz, alunite, albite, andesine, kaolinite, and a Na-Al sulfate. These mineral maps provided the basis for mapping of:

1. Opaline sinter formed by recent geyser activity.
2. Chalcedonic sinter (quartz) formed by older geyser activity.
3. Na-Al sulfates formed around active fumaroles.
4. Rocks that have undergone steam heated acid-sulfate alteration.

Vaughan et al. (2005) found that the SEBASS thermal emission data provided the unique capability for discrimination of opaline sinter, which is a primary indicator mineral characteristic of active or recently-active geothermal systems.

(Insert Figure 5)

More recently, Reath and Ramsey (2011) analyzed SEBASS data acquired during airborne surveys in 2009 and 2010 over the Salton Sea active geothermal field in California, USA. Linear spectral deconvolution (Ramsey and Christensen, 1998) was applied to the 128 long-wave infrared channels to map surface mineral assemblages associated with geothermally active areas. Mapped minerals included anhydrite, gypsum, and an unidentified sulfate mineral. Mapping results for the latter indicate variations in abundance and extent between the two data acquisitions suggesting this mineral is of a transitory nature having been formed due to surface and ground water activity. Scherer et al. (2009) integrated SEBASS with the airborne VNIR/SWIR ProspectTIR (www.spectir.com) sensor to acquire full spectrum wavelength hyperspectral data in 600 channels across the VNIR/SWIR, mid-wave, and long-wave (thermal) infrared regions for the purposes of mineral mapping. The use of this combined system provided complimentary spectral information to map a variety of minerals associated with active and recently active hydrothermal systems.

Littlefield and Calvin (2009) used MASTER data for geothermal exploration in the region of Buffalo Valley, Nevada, USA. Mineral mapping using the MASTER thermal bands discriminated silica- and clay-rich surface materials. The MASTER VNIR/SWIR bands mapped carbonate and green vegetation. Overall, the results were inconclusive in terms of identifying specific geothermal indicator minerals. Littlefield and Calvin (2009) attribute this to either the absence of these surface minerals or to the low spectral resolution of MASTER data that was unable to uniquely identify geothermal minerals.

Although ASTER's TIR data (bands 10-14) has been used to map surface temperature anomalies associated with geothermal systems (Coolbaugh et al., 2007) and for broader lithological mapping (Ninomiya et al., 2005) it has not been used extensively in the mapping of specific geothermal indicator minerals. This reflects

the low spatial (90m) and spectral resolution of this instrument that has limited potential for mapping small exposures of minerals produced by hydrothermal activity (Kruse, 2002; Littlefield and Calvin, 2009). ASTER's thermal data does have potential to contribute regional-scale information that could be used to generate exploration targets or provide context for higher spatial resolution airborne surveys. For example, Rockwell and Hofstra (2008) investigated the potential of ASTER thermal emission data to contribute to geological mapping and resource exploration studies across northern Nevada. This work analyzed a regional mosaic of ASTER thermal emission data to map quartz and carbonate minerals. For a number of localities these mineral maps corresponded to siliceous and travertine deposits associated with active hot springs.

17.6 Conclusions

TIR remote sensing provides a unique tool for qualitative and quantitative investigations of surface geothermal activity that can be applied to the exploration for new geothermal power resource and the study and monitoring of geothermal systems. Airborne broadband TIR data enables detailed mapping of discrete surface geothermal features such as hot springs and fumaroles as well as more extensive areas of thermally anomalous ground. This supports geothermal power exploration by providing a means to locate unidentified resources as well as enabling detailed mapping of known systems that can contribute to targeting and planning of field work (e.g. using maps of hot spring locations to guide water sampling). Airborne and spaceborne TIR data supports long-term monitoring of geothermal systems by providing a rapid and repeatable method of inventorying surface geothermal features. In addition, methods for relating the temperatures of surface geothermal phenomena to estimates of near-surface thermal heat loss provide important inputs to the monitoring of geothermal activity and as applied to geothermal resource assessment. The application of these methods to high resolution airborne TIR data provides estimates of conductive or convective heat loss supporting specific surface geothermal features. This information can provide system-wide estimates of near-surface heat loss, when integrated over the larger geothermal area. Time series of these data may indicate changes in geothermal activity related to deeper-seated magmatic unrest, hydrological changes, or caused by unsustainable production of developed geothermal reservoirs. The increasing availability of low-cost broadband and multispectral TIR imaging systems, Unmanned Aerial Vehicles (UAV's), and advanced image processing software (particularly for automated image registration and mosaicking) will reduce the costs of acquiring high spatial resolution airborne TIR imagery over large areas. This will support the use of airborne TIR imaging as a routine tool for exploration and monitoring of geothermal systems.

Although the spatial resolution of satellite TIR data is too coarse to investigate specific geothermal features at this time it has an important role to play in geothermal exploration and monitoring. Approaches to enhancing geothermal anomalies in TIR data have potential to facilitate the mapping of undiscovered resources, including blind systems, over large areas and at low-cost. The repeat coverage of satellite TIR sensors also provides a crucial capability for long-term monitoring studies and augments airborne surveys by providing rapid, basin-wide estimates of geothermal heat loss in a consistent and repeatable manner. Exploration and monitoring of geothermal systems will be supported by current and future satellite TIR imaging instruments. In particular, the enhanced spatial and temporal resolution of the proposed NASA HypIRI instrument has the potential to enhance monitoring capabilities.

Airborne hyperspectral thermal emission data, whilst currently not routinely used for mapping of surface mineral deposits or alteration products in support of geothermal exploration, has potential in the future to support these activities in synergy with hyperspectral VNIR/SWIR data. Hyperspectral TIR emission data provides improved capabilities over data from the VNIR/SWIR region for quantitative mapping of silicates and carbonates that may be associated with surface hydrothermal activity. This has the potential to improve the mapping of blind geothermal systems based upon the recognition of old hot spring deposits. The application of -hyperspectral TIR emission data for these purposes will be supported by the further development of instrumentation by both government and commercial organizations.

Acknowledgements

Research by the authors at Pilgrim Hot Springs, Alaska was supported by a Department of Energy Geothermal Technologies Programme (CID: DE-EE0002846; PI: Gwen Holdmann) and the Alaska Energy Authority Renewable Energy Fund Round III. We thank the anonymous reviewers for their thorough evaluation and constructive recommendations for improving this manuscript.

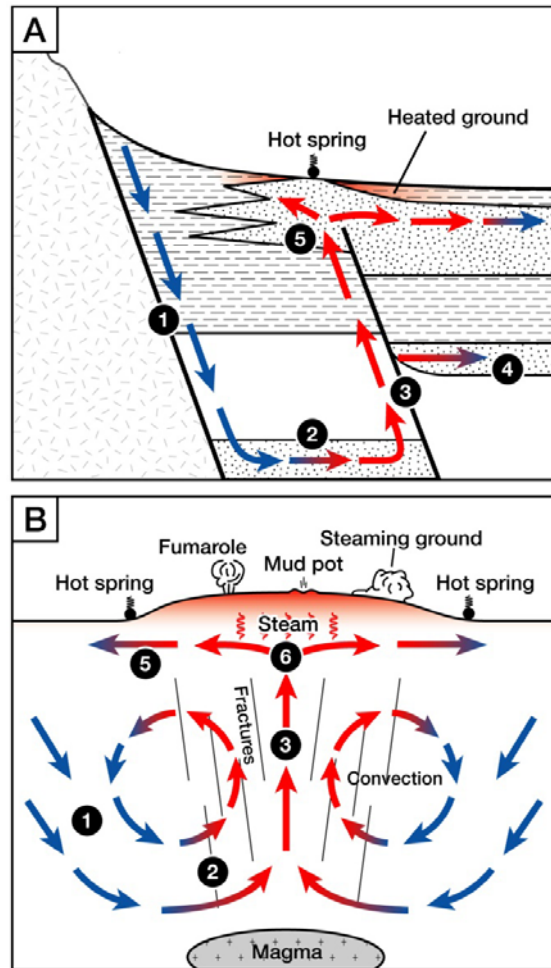


Figure 1 – Schematic diagram of geothermal systems (A) formed by deep circulation of fluids along faults and (B) related to magmatic activity. Arrows indicate direction of flow of meteoric and geothermally-heated waters. Numbers on the figure indicate: 1) zone of recharge of meteoric waters; 2) conductive heating of waters by geothermal source; 3) upflow along fault or fractures; 4) lateral outflow in deep aquifer forming a blind reservoir; 5) outflow in shallow aquifer with associated surface manifestations; 6) boiling of geothermal waters in the subsurface; source: this work.

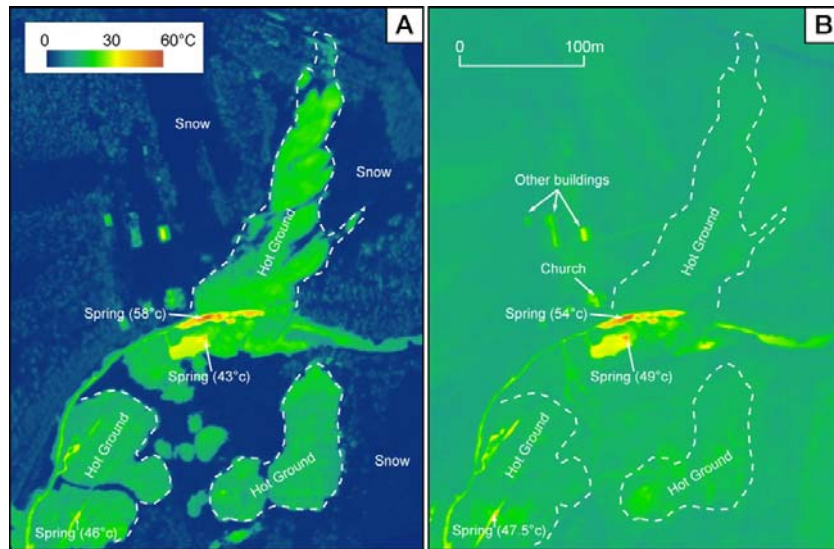


Figure 2 – Calibrated surface temperature data for part of Pilgrim Hot Springs acquired during winter 2011 (A) and fall 2010 (B) airborne surveys using a FLIR thermal camera. This data highlights the location of hot springs, hot pools and areas of heated ground as manifested in areas of anomalous snow melt in the winter 2011 data; from Haselwimmer et al., (2011).

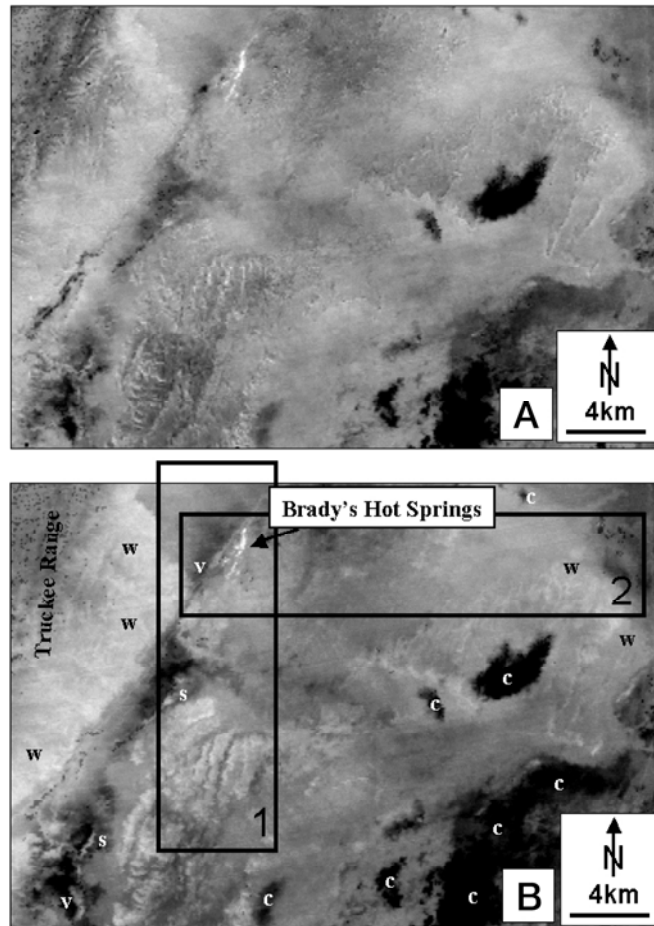


Figure 3 – ASTER day-night image for the Brady's Hot Springs area processed to minimize variations in temperature related to albedo, topographic slope/aspect, and thermal inertia (A) and unprocessed ASTER nighttime surface kinetic temperature (AST08) image (B). Around 34-53% of temperature variation in (B) has been removed in (A) as evidenced from the variances in temperature of the areas encompassed in boxes 1 and 2. This processing has resulted in the Fumaroles at Brady's Hot Springs being more readily discernible. Abbreviations: c = clouds, s = ground water springs, v = vegetation, W = 'warm' ground; adapted from Coolbaugh et al., (2007)

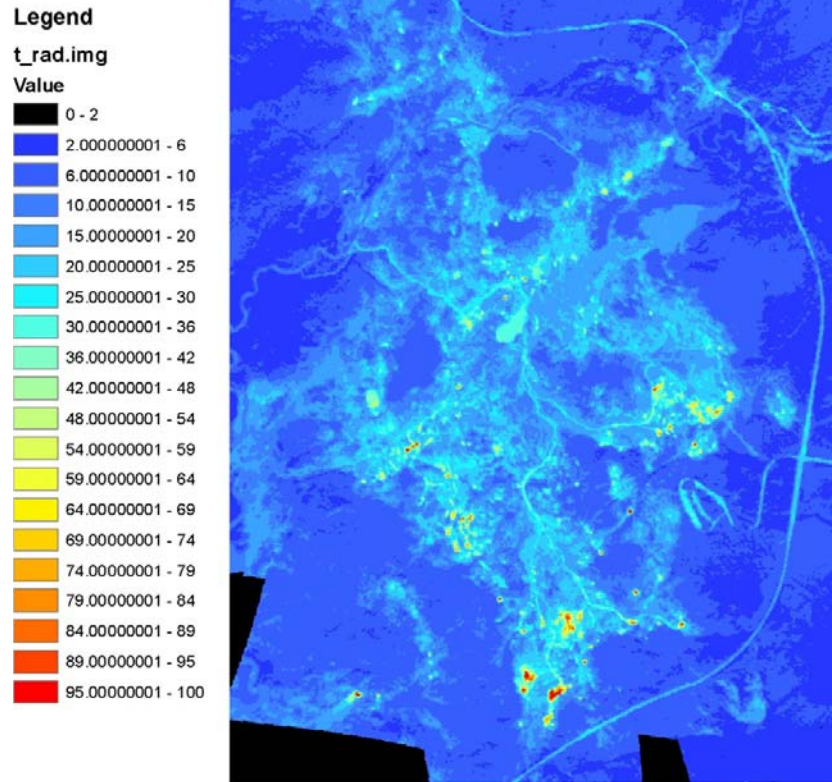


Figure 4 – Radiant temperature values (in degrees C) for Norris Geyser Basin acquired on October 06, 2005 between 1-3pm using ASD SpectraView system; from Seielstad and Queen (2009).

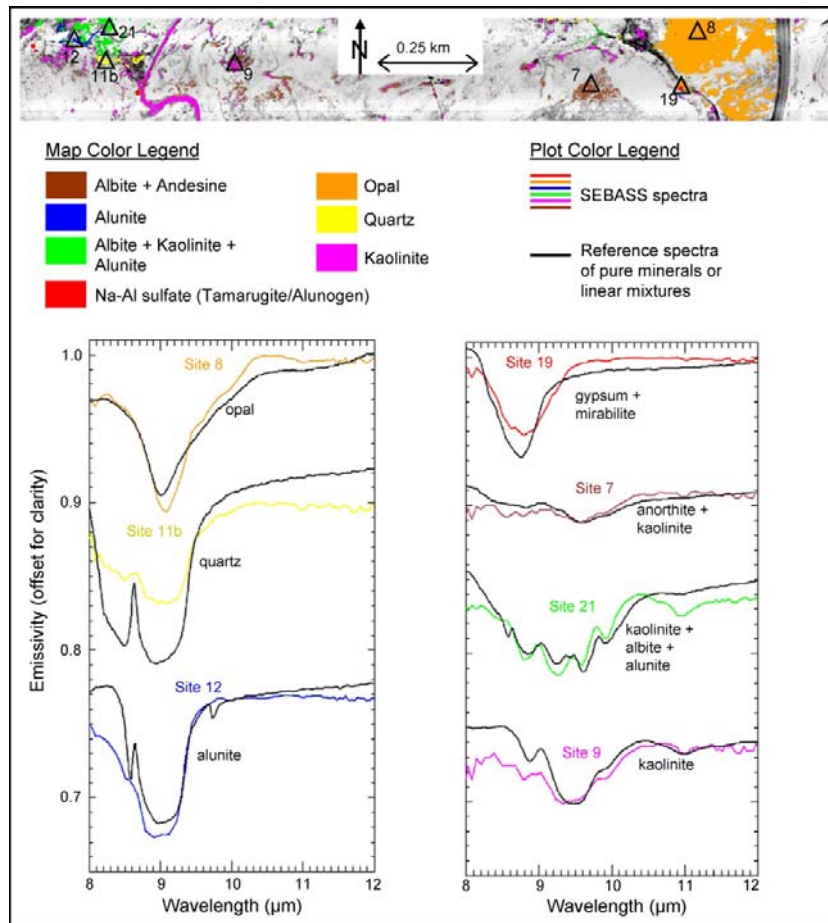


Figure 5 – Top: results of mineral mapping using SEBASS data for Steamboat Springs - mapped minerals are shown in the different colors overlaid onto a gray-scale emissivity image. Bottom: SEBASS spectra (colored lines) for the field localities indicated by triangles on the mineral map shown next to pure and mixed mineral library spectra (black lines); from Vaughan et al., (2005).

References

- Allis, R. G. (1980). "Changes in heat flow associated with exploitation of Wairakei geothermal field, New Zealand." New Zealand Journal of Geology and Geophysics **24**: 1-19.
- Allis, R. G., G. D. Nash and S. D. Johnson (1999). "Conversion of thermal infrared surveys to heat flow: Comparisons from Dixie Valley, Nevada, and Wairakei, New Zealand." GRC Transactions **23**.
- Baldrige, A. M., S. J. Hook, C. I. Grove and G. Rivera (2009). "The ASTER spectral library version 2.0." Remote Sensing of Environment **113**(4): 711-715.
- Berk, A., L. S. Bernstein and D. C. Robertson (1989). MODTRAN: A moderate resolution model for LOWTRAN7. GL-TR-89-0122. Bedford, MA: Air Force Geophysics Lab.
- Bromley, C. J., S. M. van Manen and D. Graham (2010). Monitoring surface geothermal features using time series of aerial and ground-based photographs. American Geophysical Union, Fall Meeting 2010, abstract #IN33B-1308, San Francisco.
- Bromley, C. J., S. M. van Manen and W. Mannington (2011). Heat flux from steaming ground: reducing uncertainties. Thirty-Sixth Workshop on Geothermal Reservoir Engineering, Stanford University, Stanford, California.
- Carter, A. J., O. Girina, M. S. Ramsey and Y. V. Demyanchuk (2008). "ASTER and field observations of the 24 December 2006 eruption of Bezymianny Volcano, Russia." Remote Sensing of Environment **112**(5): 2569-2577.
- Christensen, P. R., J. L. Bandfield, V. E. Hamilton, D. A. Howard, M. D. Lane, J. L. Piatek, S. W. Ruff and W. L. Stefanov (2000). "A thermal emission spectral library of rock-forming minerals." J. Geophys. Res. **105**(E4): 9735-9739.
- Coolbaugh, M. F., C. Kratt, A. Fallacaro, W. M. Calvin and J. V. Taranik (2007). "Detection of geothermal anomalies using Advanced Spaceborne Thermal Emission and Reflection Radiometer (ASTER) thermal infrared images at Bradys Hot Springs, Nevada, USA." Remote Sensing of Environment **106**(3): 350-359.
- Coolbaugh, M. F. and L. A. Shevenell (2004). "A method for estimating undiscovered geothermal resources in Nevada and The Great Basin." GRC Transactions **28**: 13-18.
- DiPippio, R. (2005). Geothermal Power Plants: Principles, Applications and Case Studies, Elsevier.

- Eneva, M. and M. Coolbaugh (2009). "Importance of Elevation and Temperature Inversions for the Interpretation of Thermal Infrared Satellite Images Used in Geothermal Exploration." GRC Transactions **33**.
- Eneva, M., M. Coolbaugh and J. Combs (2006). "Application of Satellite Thermal Infrared Imagery to Geothermal Exploration in East Central California." GRC Transactions **30**.
- Eneva, M., M. F. Coolbaugh and S. J. Bjornstad (2007). In search for thermal anomalies in the coso geothermal field (California) using remote sensing and field data. Thirty-Second Workshop on Geothermal Reservoir Engineering, Stanford University, Stanford, California.
- Fridleifsson, I. B., R. Bertani, E. Huenges, J. W. Lund, A. Ragnarsson and L. Rybach (2008). The possible role and contribution of geothermal energy to the mitigation of climate change. IPCC Scoping Meeting on Renewable Energy Sources, Luebeck, Germany.
- Gillespie, A., S. Rokugawa, T. Matsunaga, J. S. Cothem, S. Hook and A. B. Kahle (1998). "A temperature and emissivity separation algorithm for Advanced Spaceborne Thermal Emission and Reflection Radiometer (ASTER) images." IEEE transactions on geoscience and remote sensing **36**(4): 1113-1126.
- Glassley, W. E. (2010). Geothermal Energy: Renewable Energy and the Environment, CRC Press.
- Hackwell, J. A., D. W. Warren, R. P. Bongiovi, S. J. Hansel, T. L. Hayhurst, D. J. Mabry, M. G. Sivjee and J. W. Skinner (1996). LWIR/MWIR imaging hyperspectral sensor for airborne and ground-based remote sensing, SPIE.
- Hapke, B. (1993). Theory of Reflectance and Emittance Spectroscopy. Cambridge, Cambridge University Press.
- Haselwimmer, C. E. and A. Prakash (2011). Use of airborne thermal imaging to quantify heat flux and flow rate of surface geothermal fluids at Pilgrim Hot Springs, Alaska. AGU Fall Meeting 2011, San Francisco.
- Haselwimmer, C. E., A. Prakash and G. Holdmann (2011). Geothermal Exploration at Pilgrim Hot Springs, Alaska Using Airborne Thermal Infrared Remote Sensing. Geothermal Resource Council Annual Meeting 2011, San Diego.
- Heasler, H., C. Jaworowski and D. Foley (2009). Geothermal systems and monitoring hydrothermal features. Geological Monitoring. R. Young and L. Norby. Boulder, Colorado, Geological Society of America.
- Hellman, M. J. and M. S. Ramsey (2004). "Analysis of hot springs and associated deposits in Yellowstone National Park using ASTER and AVIRIS remote sensing." Journal of Volcanology and Geothermal Research **135**(1-2): 195-219.
- Hodder, D. T. (1970). "Application of remote sensing to geothermal prospecting." Geothermics **2, Part 1**(0): 368-380.

- Hook, S. J., J. J. Myers, K. J. Thome, M. Fitzgerald and A. B. Kahle (2001). "The MODIS/ASTER airborne simulator (MASTER) — a new instrument for earth science studies." Remote Sensing of Environment **76**(1): 93-102.
- Hunt, G. R. (1977). "Spectral signatures of particulate minerals in the visible and near infrared." Geophysics **42**(3): 501-513.
- Huntington, J. F. (1996). The Role of Remote Sensing in Finding Hydrothermal Mineral Deposits on Earth. Ciba Foundation Symposium 202 - Evolution of Hydrothermal Ecosystems on Earth (And Mars?), John Wiley & Sons, Ltd.: 214-235.
- Johnson, B. R. (1998). In scene atmospheric compensation: Application to SEBASS data collected at the ARM site. Part 1. Aerospace corporation technical report, ATR-99 (8407)-1.
- Kealy, P. S. and A. R. Gabell (1990). "Estimation of emissivity and temperature using alpha coefficients." In Proceedings of the Second TIMS Workshop, JPL Publication **90**: 55.
- Kienholz, C., A. Prakash and A. Kolker (2009). Geothermal Exploration in Akutan, Alaska, Using Multitemporal Thermal Infrared Images. American Geophysical Union, Fall Meeting 2009, , abstract #H53F-1009.
- Kratt, C., W. Calvin and M. Coolbaugh (2006). "Geothermal exploration with Hymap hyperspectral data at Brady–Desert Peak, Nevada." Remote Sensing of Environment **104**(3): 313-324.
- Kratt, C., M. F. Coolbaugh and W. M. Calvin (2006). "Remote Detection of Quaternary Borate Deposits with ASTER Satellite Imagery as a Geothermal Exploration Tool." GRC Transactions **30**.
- Kruse, F. A. (2002). Combined SWIR and LWIR mineral mapping using MASTER/ASTER. Geoscience and Remote Sensing Symposium, 2002. IGARSS '02. 2002 IEEE International.
- Kruse, F. A., J. W. Boardman and J. F. Huntington (2003). "Comparison of airborne hyperspectral data and EO-1 Hyperion for mineral mapping." Geoscience and Remote Sensing, IEEE Transactions on **41**(6): 1388-1400.
- Lee, K. (1978). "Analysis of thermal infrared imagery of the Black Rock Desert geothermal area." Journal Name: Q. Colo. Sch. Mines; (United States); Journal Volume: 73:3; Medium: X; Size: Pages: 31-43.
- Littlefield, E. and W. Calvin (2009). "Remote Sensing for Geothermal Exploration Over Buffalo Valley, NV." GRC Transactions **33**: 495-499.
- Littlefield, E. and W. Calvin (2010). "Geothermal Exploration using AVIRIS Remote Sensing Data over Fish Lake Valley." GRC Transactions **34**: 599-603.
- Mongillo, M. (1994). "Aerial Thermal Infrared Mapping of the Waimangu-Waiotapu Geothermal Region, New Zealand." Geothermics **23**(5/6): 511-526.
- Mongillo, M. A. and D. J. Graham (1999). Quantitative evaluation of airborne video TIR survey imagery. 21st New Zealand Geothermal Workshop.

- Nash, G. D., G. W. Johnson and S. Johnson (2004). "Hyperspectral detection of geothermal system-related soil mineralogy anomalies in Dixie Valley, Nevada: a tool for exploration." Geothermics **33**(6): 695-711.
- Ninomiya, Y., B. Fu and T. J. Cudahy (2005). "Detecting lithology with Advanced Spaceborne Thermal Emission and Reflection Radiometer (ASTER) multispectral thermal infrared "radiance-at-sensor" data." Remote Sensing of Environment **99**(1-2): 127-139.
- Pieri, D. and M. Abrams (2004). "ASTER watches the world's volcanoes: a new paradigm for volcanological observations from orbit." Journal of Volcanology and Geothermal Research **135**(1-2): 13-28.
- Ramsey, M. S. and P. R. Christensen (1998). "Mineral abundance determination: Quantitative deconvolution of thermal emission spectra." J. Geophys. Res. **103**(B1): 577-596.
- Reath, K. A. and M. S. Ramsey (2011). Hyperspectral Thermal Infrared Analysis of the Salton Sea, CA Geothermal Field. AGU Fall Meeting 2011. San Francisco.
- Riley, D. N., W. A. Peppin, G. P. Bryant and C. Wright (2008). Joint Airborne Collection of Hyperspectral Systems: Mineral Mapping in Cuprite in VNIR-SWIR and MWIR-LWIR with 613 spectral channels. Annual General Meeting of the Geological Remote Sensing Group 2008. London.
- Rockwell, B. W. and A. H. Hofstra (2008). "Identification of quartz and carbonate minerals across northern Nevada using ASTER thermal infrared emissivity data—Implications for geologic mapping and mineral resource investigations in well-studied and frontier areas." Geosphere **4**(1): 218-246.
- Rybach, L. (1981). Geothermal Systems, Conductive Heat Flow, Geothermal Anomalies. Geothermal Systems: Principles and Case Histories. L. Rybach and L. J. P. Muffler, John Wiley & Sons.
- Scherer, G. J., D. N. Riley, W. A. Peppin, D. M. Tratt, C. Wright and K. L. Jones (2009). Geothermal Exploration with Visible through Long Wave Infrared Imaging Spectrometers. Clean Technology 2009. Houston, Texas.
- Seielstad, C. and L. Queen (2009). Thermal Remote Monitoring of the Norris Geyser Basin, Yellowstone National Park. Final Report for the National Park Service Cooperative Ecosystem Studies Unit, Agreement No. H1200040001: 38 pp.
- Taranik, J. V., M. F. Coolbaugh and R. G. Vaughan (2009). An Overview of Thermal Infrared Remote Sensing with Applications to Geothermal and Mineral Exploration in the Great Basin, Western United States. In Reviews in Economic Geology, v.16, : Remote Sensing and Spectral Geology. R. Bedell, A. Crosta and E. Grunsky. Littleton, CO, Society of Economic Geologists Inc.

- Vaughan, R. G., W. M. Calvin and J. V. Taranik (2003). "SEBASS hyperspectral thermal infrared data: surface emissivity measurement and mineral mapping." Remote Sensing of Environment **85**(1): 48-63.
- Vaughan, R. G., S. J. Hook, W. M. Calvin and J. V. Taranik (2005). "Surface mineral mapping at Steamboat Springs, Nevada, USA, with multi-wavelength thermal infrared images." Remote Sensing of Environment **99**(1-2): 140-158.
- Vaughan, R. G., L. P. Keszthelyi, J. B. Lowenstern, H. Heasler and C. Jaworowski (2011). Measuring and Monitoring Heat Flow and Hydrothermal Changes in the Yellowstone Geothermal System using ASTER and MODIS Thermal Infrared Data. AGU Fall Meeting 2011. San Francisco.
- Watson, F. G. R., R. E. Lockwood, W. B. Newman, T. N. Anderson and R. A. Garrott (2008). "Development and comparison of Landsat radiometric and snowpack model inversion techniques for estimating geothermal heat flux." Remote Sensing of Environment **112**(2): 471-481.
- Wisian, K. W., D. D. Blackwell and M. Richards (2001). "Correlation of Surface Heat Loss and Total Energy Production for Geothermal Systems." Geothermal Resources Council Transactions **25**.